Advances in the Physics Basis of the Hybrid Scenario on DIII-D

C.C. Petty 1), W.P. West 1), J.C. DeBoo 1), E.J. Doyle 2), T.E. Evans 1),
M.E. Fenstermacher 3), M. Groth 3), J.R. Ferron 1), G.R. McKee 4), P.A. Politzer 1),
L. Schmitz 2), S.L. Allen 3), M.E. Austin 5), N.H. Brooks 1), T.A. Casper 3), M.S. Chu 1),
C.M. Greenfield 1), C.T. Holcomb 3), A.W. Hyatt 1), G.L. Jackson 1), J.E. Kinsey 1),
R.J. La Haye 1), T.C. Luce 1), M.A. Makowski 3), R.A. Moyer 6), M. Murakami 7),
T.H. Osborne 1), T.L. Rhodes 2), M.R. Wade 1), and G. Wang 2)

1) General Atomics, P.O. Box 85608, San Diego, California, 92186-5608, USA
2) University of California-Los Angeles, Los Angeles, California 90095, USA
3) Lawrence Livermore National Laboratory, Livermore, California 94550, USA
4) University of Wisconsin-Madison, Madison, Wisconsin 53706, USA
5) University of Texas-Austin, Austin, Texas 78712, USA
6) University of California-San Diego, San Diego, California 92093, USA
7) Oak Ridge National Laboratory, Oak Ridge, Tennessee 37831, USA

e-mail contact of main author: petty@fusion.gat.com

Abstract. Recent experiments on DIII-D have extended the hybrid scenario towards the burning plasma regime by incorporating strong electron heating, low torque injection, and edge localized mode (ELM) suppression. Hybrid performance projecting to $Q \geq 10$ on ITER at $q_{95}=3.1$ has been achieved in plasmas with reduced ion/electron temperature ratio or Mach number. Confinement is decreased relative to previous hybrid results, consistent with measurements of increased turbulence at low and intermediate wavenumbers. For the first time, large type-I ELMs have been completely suppressed in a hybrid plasma at $q_{95}=3.6$ by applying edge resonant magnetic perturbations (RMPs) with toroidal mode number $n=3$. Additionally, high performance hybrid and steady-state scenario operation has been demonstrated with reduced frequency of wall conditioning with a >95% graphite plasma-facing wall.

1. Introduction

Experiments on the DIII-D tokamak have developed a long duration, high performance plasma discharge that is an attractive operating scenario for future burning plasma experiments [1,2]. In contrast to steady-state scenarios, this "hybrid scenario" has <100% noninductive current fraction, with bootstrap current fractions of 35%–50% and a central safety factor close to unity. Similar realizations of the hybrid scenario have been reported from the ASDEX-U [3], JET [4], and JT-60U [5] tokamaks. Although hybrid plasmas normally have type-I edge localized modes (ELMs), like the standard H-mode scenario, hybrids differ by having suppressed or reduced amplitude sawteeth (depending on q_{95}), a higher β limit to the m/n=2/1 neoclassical tearing mode (NTM), and remarkably good transport properties. While hybrid plasmas on DIII-D typically have a small m/n=3/2 NTM, some hybrid discharges develop a m/n=4/3 or 5/3 NTM instead, which results in higher confinement but without the sawtooth suppression. Recent experiments on DIII-D have extended the hybrid scenario towards the burning plasma regime by incorporating strong electron heating, low torque injection, and ELM suppression from edge resonant magnetic perturbations (RMPs) in an ITER-similar shape. These experiments show that the beneficial characteristics of the hybrid scenario are maintained under these "burning plasma relevant" conditions. With >95% graphite plasma-facing surfaces on DIII-D, the capability to obtain high performance plasmas in both the hybrid and steady-state scenarios has been demonstrated over extended operational periods with no intervening boronizations.

Additionally, with strong divertor pumping, density control can be maintained over many discharges with no between-shot helium glow discharge cleaning.

2. Dependence of Transport on Ion/Electron Temperature Ratio

Initial hybrid experiments on DIII-D using co-neutral beam injection (NBI) as the only source of auxiliary heating obtained ion temperatures (T_i) significantly above electron temperatures (T_e) and high toroidal rotation velocities (V_{tor}) [1,2], which are plasma conditions quite different from those expected in ITER. Since $T_i > T_e$ has been shown to be favorable for transport [6], the role of the ion/electron temperature ratio in achieving good confinement in hybrids needs to be examined before extrapolating the results to a burning plasma. Previous density scans in hybrids on DIII-D showed a modest decrease in the thermal energy confinement time (<10%) as T_i/T_e was lowered from 1.9 to 1.5 [7,8]. However, as these experiments varied T_i/T_e and collisionality (ν_*) simultaneously, both of which are known to affect transport [9,10], additional studies were needed to isolate the effect of T_i/T_e alone.

Recent hybrid experiments on DIII-D have replaced some of the co-NBI heating with electron cyclotron heating (ECH) at constant density to raise T_e closer to T_i. Using four 110 GHz gyrotrons with 2.4 MW of total injected power, separate trials with either 3rd harmonic or 2nd harmonic ECH found that raising T_e/T_i reduces energy confinement, similar to the result in standard H-mode plasmas [9]. Since electron heating is also observed to decrease the toroidal rotation at fixed injected torque, comparison discharges without ECH, but at the same normalized beta (β_N) and density, have been produced using a mix of co- and counter-NBI to match V_{tor}. A comparison of hybrid discharges (β_N=2.6, q_{95}=3.3) with and without ECH is shown in Fig. 1, where 3rd harmonic damping is utilized with a calculated

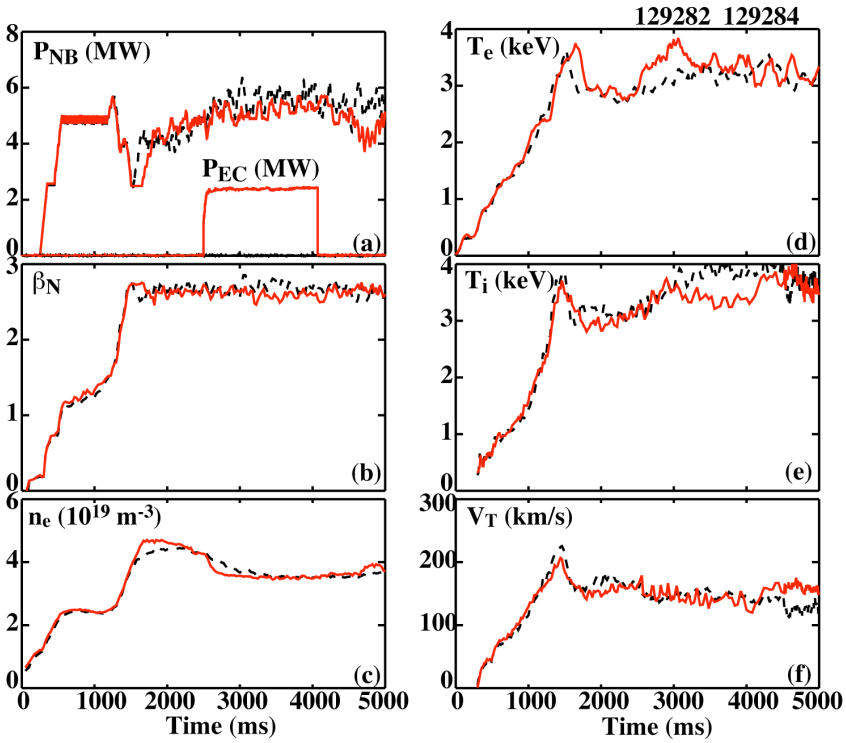

FIG. 1. Time history of matched hybrid plasmas with (red solid) and without (black dash) 3rd harmonic ECH. (a) NBI and ECH powers, (b) normalized beta, (c) line-average density, (d) electron temperature at ρ≈0.32, (e) ion temperature at ρ≈0.39, and (f) toroidal rotation velocity at ρ≈0.39.

first pass absorption of 94%. The effect of ECH is to decrease T_i/T_e by ≈20%, bringing the volume-average value down to ≈1.07. The thermal energy confinement time, normalized to the IPB98(y,2) scaling relation [11], decreases from H_{98y2}=1.22 to 1.07 with ECH. Power balance transport analysis using the ONETWO code [12] shows that this confinement decrease comes from an increase in both electron and ion heat conduction. A radial average of the transport results between ρ=0.5 and 0.7, where ρ is the normalized toroidal flux coordinate, finds that ECH causes the electron thermal diffusivity to increase from χ_e=1.5 m^2s^{-1} to 3.9 m^2s^{-1}, and the ion thermal diffusivity to increase from χ_i=1.7 m^2s^{-1} to 2.9 m^2s^{-1}.

The increase in transport with strong electron heating in hybrid plasmas correlates with increased density turbulence at low and intermediate wavenumbers. Figure 2 shows the power spectrum measured by beam emission spectroscopy (BES) at a radius of ρ=0.7 for the same two discharges in Fig. 1. The BES diagnostic measures long-wavelength density fluctuations with wavenumbers <3 cm^{-1} [13]. The amplitude of the turbulence in Fig. 2 clearly increases with ECH. As the frequency dependence of the power spectrum is dominated by the Doppler shift from the bulk plasma rotation, the self-similar shapes seen in Fig. 2 confirm that the toroidal rotation is held fixed. The density fluctuation spectrum has also been probed at intermediate wavenumber (near 7–8 cm^{-1}) using Doppler backscattering (DBS) [14]. As seen in Fig. 3, the density fluctuation amplitude measured around ρ=0.6–0.7 increases during ECH. The spikes in the density fluctuation amplitude are caused by ELMs shifting the probing location transiently to larger ρ.

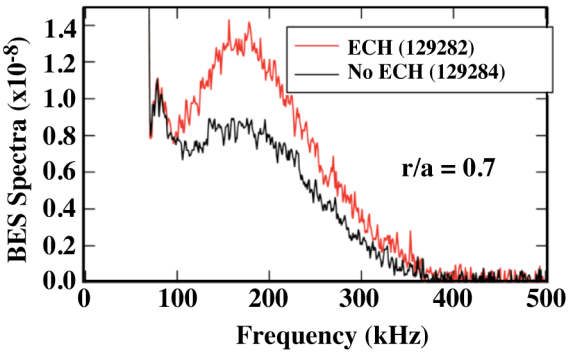

FIG. 2. Fluctuation power spectrum measured by BES with (red) and without (black) 2.4 MW of ECH in β_N=2.6 hybrid plasmas.

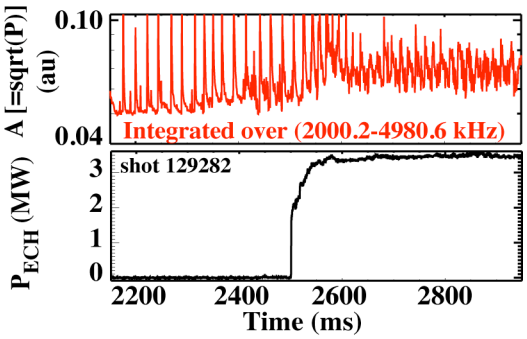

FIG. 3. Time history of integrated power spectrum of density fluctuations around ρ=0.6-0.7 measured by DBS for hybrid plasma with 2.4 MW of ECH. The noise floor for the fluctuation amplitude is ≈0.05.

Theory-based transport modeling confirms that strong electron heating should increase the turbulent transport in these hybrid plasmas. Linear calculations using the trapped gyro-Landau-fluid (TGLF) model [15] show that the most unstable growth rate at ρ=0.5 is more than 50% larger for the hybrid plasma with ECH compared to the one without ECH. The peak growth rates occur around $k_\theta\rho_s$≈0.4, where k_θ is the poloidal wavenumber, $\rho_s=c_S/\Omega_I$, c_S is the sound speed, and Ω_i is the ion cyclotron frequency, with rotation in the ion diamagnetic direction. Further from the axis (ρ=0.7), the short-wavelength electron temperature gradient (ETG) mode is also predicted to be unstable for both the with-ECH and without-ECH hybrids. Closer to the axis (ρ=0.3), the calculated growth rates from TGLF are small for both cases.

3. Dependence of Transport on Toroidal Mach Number

Extrapolating the hybrid scenario with co-NBI to ITER is not straightforward because the large amount of injected angular momentum results in a Mach number ($M_\phi=V_{tor}/c_S$) several times greater than expected for ITER. Since rapid rotation is known to improve the plasma confinement [16] and stability properties [17], experiments on DIII-D have studied the characteristics of the hybrid scenario in plasmas with reduced values of the Mach number by utilizing nearly balanced beam injection [18]. Hybrid plasmas with co-NBI have peaked toroidal rotation profiles with a central Mach number near $M_\phi\approx0.4$, while for nearly balanced-NBI the toroidal rotation profile becomes flat and the Mach number can be reduced to $M_\phi\approx0.04$. Experiments on DIII-D find that the beneficial characteristics of the hybrid scenario are maintained with low torque injection; for example, sawteeth remain suppressed and the stability limit for m/n=2/1 NTM is at least β_N=3.0. As the toroidal rotation velocity is reduced by shifting from co-NBI to nearly balanced-NBI, the confinement factor is reduced from $H_{98y2}\geq1.4$ to a value of $H_{98y2}\geq1.1$, as good as conventional H-mode plasmas with strong rotation. Modeling using the TGLF and GLF23 transport simulation codes shows the increase in heat transport with lower NBI torque is consistent with the effects of the change in the E×B flow shear [18,19].

Hybrid plasmas on DIII-D at q_{95}=3.1 with low amounts of injected torque, but with T_i above T_e by 30%, achieve conditions consistent with $Q\geq10$ on ITER. Figure 4 plots a hybrid discharge that transitions from co-NBI startup to more balanced-NBI at the initiation of the high β_N phase (2000 ms). The fusion performance factor, $\beta_N H_{89}/q_{95}^2$, for this plasma exceeds the value required for Q=10 operation on ITER for more than four current redistribution times (τ_R). Extrapolating this hybrid discharge to ITER at 15 MA of plasma current leads to a projection of Q slightly above 10 either assuming a fixed H_{98y2} or H_{89} confinement factor, where the later is the energy confinement time normalized to the ITER89P L-mode scaling relation. Projections using a confinement scaling relation consistent with transport mechanisms that are electrostatic and gyroBohm-like [20] results in a prediction of ignition for this hybrid plasma on ITER. Therefore, DIII-D experiments with low values of the Mach number and an ITER-similar plasma shape have shown that the hybrid scenario continues to meet or exceed the fusion performance requirements of the ITER project.

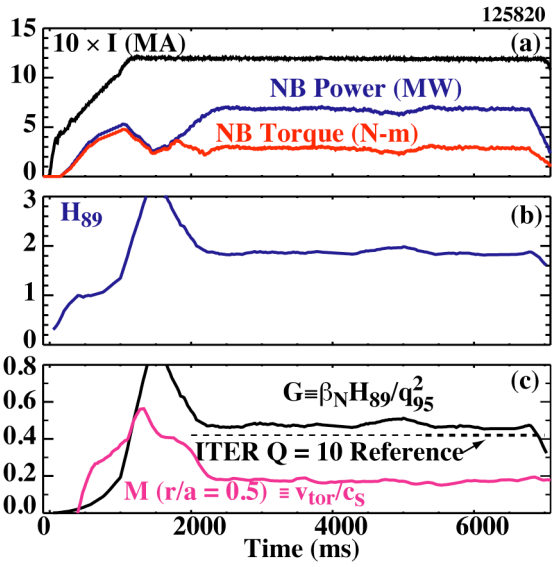

FIG. 4. Time history of high-performance hybrid with low toroidal rotation. (a) Plasma current, NBI power and torque, (b) normalized beta, and (c) fusion performance factor and Mach number at mid-radius.

4. Complete ELM Suppression using n=3 RMP

For the first time, large type-I ELMs have been completely suppressed in hybrid plasmas by applying edge RMPs using the DIII-D I-coil with toroidal mode number n=3. This is an

important advance in developing hybrid discharges as a baseline-operating scenario for ITER because such ELMs may cause unacceptable divertor erosion. This work builds upon the successful use of edge RMPs to suppress ELMs in the low ν_*, standard H-mode regime [21]. Analysis of the edge profiles has shown that the RMP enhances particle transport, reducing the H-mode pedestal density and pressure gradient such that the edge plasma becomes stable to the peeling-ballooning modes that drive the ELMs.

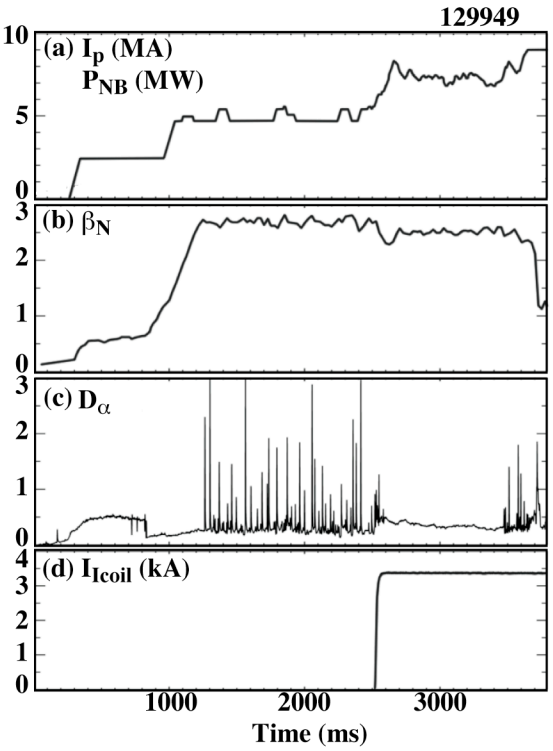

FIG. 5. ELM suppression by n=3 RMP: (a) NBI power, (b) normalized beta, (c) divertor D_α recycling signal, and (d) RMP coil current.

In Fig. 5, type-I ELMs are eliminated shortly after the RMP coil is turned on in hybrid plasmas with β_N=2.5, q_{95}=3.6, and a lower single-null divertor shape similar to ITER. This low-ν_* hybrid discharge has a m/n=4/3 NTM and occasional sawteeth. The choice of edge safety factor is important since previous research on DIII-D found that ELM suppression during n=3 RMP application is a resonant effect. For the discharge in Fig. 5, an I-coil current of 3.4 kA corresponds to a normalized m/n=11/3 magnetic field perturbation of $\delta B_r/B_t=3.9\times10^{-4}$. The high performance phase of the plasma shown in Fig. 5 ends after half a current diffusion time (where τ_R=1.9 s during the I-coil phase) when a fishbone-triggered m/n=3/2 NTM grows and locks to the vessel wall. A rapid decrease in the m/n=3/2 NTM frequency from 13 kHz to ~0 occurs after 3.5 s and is correlated with the reappearance of small ELMs. While the reason for the initial slowing of the m/n=3/2 NTM is not understood, once the frequency drops below ≈6 kHz the drag from the induced wall eddy current is calculated to be sufficient to cause locking [22,23]. The I-coil RMP does not result in locking for hybrid plasmas with a m/n=4/3 NTM, and locking is avoided for the m/n=3/2 NTM case at lower β_N (discussed below). During the ELM suppressed phase, the fusion performance factor is equal to the value needed to obtain Q=10 operation on ITER in the baseline scenario.

The largest effect of the I-coil on the plasma profiles is a global decrease in density, with a concomitant increase in temperature (since β_N is kept constant by the plasma control system). The toroidal rotation is reduced as a consequence of the non-resonant and resonant braking effects of non-axisymmetric magnetic fields [24], which is likely responsible for the drop in thermal energy confinement factor from H_{98y2}=1.35 to H_{98y2}=1.05. Although the m/n=4/3 NTM island width increases with reduced flow shear, it is too small to significantly affect global confinement. A power balance transport analysis using the ONETWO code shows that χ_e increases by 2× at all radii during the ELM suppression phase. While χ_i increases by 2× in the outer half of the plasma, it is nearly unchanged in the inner half as the reduction in flow shear is apparently offset by the developing hot ion mode. This measured rise in heat transport during ELM suppression agrees with changes in the calculated

turbulence growth rates using the TGLF theory-based transport code. Comparing similar hybrid plasmas with and without I-coil, TGLF predicts that the ELM suppressed case should have 2× larger growth rates for modes between $0.1<k_\theta\rho_s<1$ at $\rho=0.5$, and 3× larger growth rates for shorter wavelength modes at $\rho=0.7$.

Complete ELM suppression with the I-coil RMP is also obtained for hybrid plasmas with a $m/n=3/2$ NTM (which is the more usual mode on DIII-D) for $\beta_N\leq 2.2$ for up to one current diffusion time ($\tau_R=1.5$ s during the I-coil phase). A strong coupling between the $m/n=3/2$ NTM and the $m/n=2/2$ sideband near the axis can occur in these hybrids, which flattens the toroidal rotation profile between the $q=1$ and $q=1.5$ surfaces. This results in a sudden increase in the $m/n=3/2$ NTM amplitude, and the mode frequency drops to a value just above the critical level for locking (≈6 kHz). While complete ELM suppression is also obtained for $\beta_N\approx 2.4$ in $m/n=3/2$ NTM hybrids, the application of the I-coil causes the $m/n=3/2$ mode amplitude to double and the toroidal rotation rate to quickly drop below the critical level, which is followed by mode locking. The strong dependence on β_N may be due to resonant field amplification of non-axisymmetric magnetic fields, which increases both the non-resonant and resonant braking by the I-coil RMP. However, it is not clear why hybrids with a $m/n=3/2$ NTM rotate more slowly (thus becoming more susceptible to locking) during I-coil application than hybrids with a $m/n=4/3$ NTM. An obvious approach to overcoming this β_N limit in ELM suppressed hybrids is to use electron cyclotron current drive (ECCD) aimed at the $q=1.5$ surface to control the size of the $m/n=3/2$ mode. This ECCD capability exists on DIII-D and will be available on ITER.

5. Dependence on Wall Conditioning

Recent experiments on DIII-D, with >95% graphite plasma-facing surfaces, have demonstrated the capability to obtain high performance plasmas, in both hybrid ($\beta_N H_{89}\sim 6$) and steady-state ($\beta_N H_{89}\sim 9$) scenarios, over extended operational periods (three months or >6000 plasma seconds) during each of the 2006 and 2007 campaigns with no intervening boronizations (BZN) [25]. BZNs [26] were performed at the beginning and near the end of the 2006 campaign on DIII-D. Benchmark hybrid and steady-state scenario discharges were reproduced soon after the initial BZN, and again prior to and just after the second BZN. Figure 6 shows performance data, including β_N, H_{89}, and the fusion performance factor ($\beta_N H_{89}/q_{95}^2$) from four hybrid discharges taken during the 2006–2007 campaigns, and demonstrates that special wall conditioning is not required on DIII-D to operate high-confinement, high-beta plasmas over a long campaign. Discharge 127671 was taken near the beginning of the 2007 campaign, after a six-week long entry vent but *prior* to the first and only BZN of the year. Steady-state scenario discharges taken across the 2006 campaign show a similar level of repeatability in performance parameters.

With the strong divertor pumping used in the hybrid discharges, good performance can be maintained over several sequential discharges with no between-shot helium glow discharge cleaning [27]. Between shots 126479 and 126485, shown in Fig. 6, there was no between-shot helium glow discharge cleaning. In these discharges, control of the density (not shown) is well maintained.

Over the same period, impurity influx and net plasma fueling were monitored with daily reference shots. Figure 7 shows the trends in charge exchange line emission from core carbon, the edge line emission from C^{+2}, the net fueling to reach the target L-mode density,

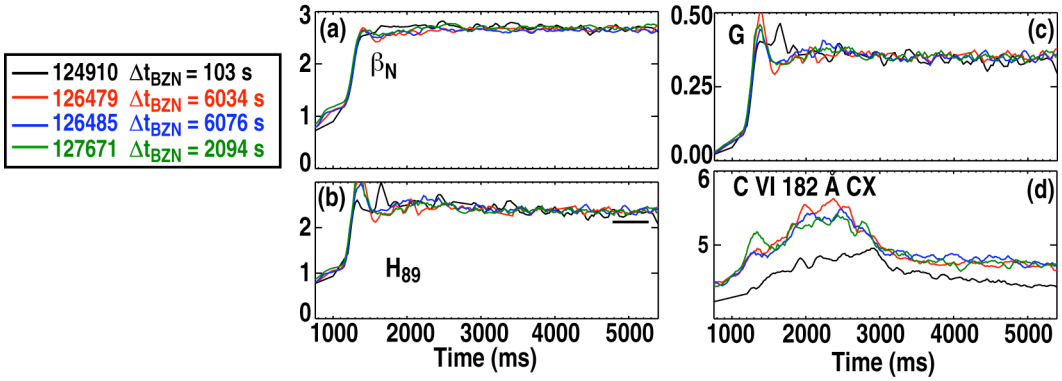

FIG. 6. Time histories of the (a) normalized beta, (b) H-mode confinement factor relative to ITER89P L-mode scaling, (c) fusion performance factor ($\beta_N H_{89}/q_{95}^2$), and (d) core carbon charge exchange emission from four hybrid discharges from the 2006 and 2007 campaigns are shown. The plasma operating time since the most recent boronization is shown in the legend (Δt_{BZN}).

and the peak time rate of change of the density immediately after the L-H transition in these reference shots as a function of the total plasma operating time since the last BZN. Core and edge emission from carbon, the dominant impurity on DIII-D, rises immediately after a BZN, then saturates and shows no secular trend for several thousand plasma seconds of operation. No secular trends are seen in the gas puffing necessary to reach the target density or in the wall fueling of the ELM-free H-mode period immediately following the L-H transition.

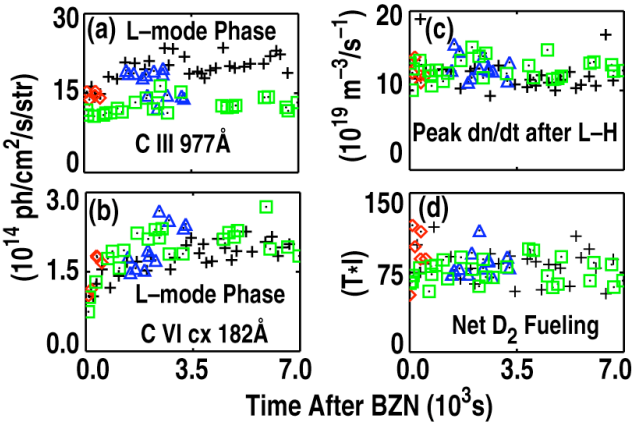

FIG. 7. Impurity and particle source related measurements from the daily references shots over the 2006 campaign (black plusses-after first BZN and red diamonds after the second BZN) and 2007 campaign (blue triangles after the 6 week entry vent and green squares after the first and only BZN).

These findings on DIII-D, which has a >95% graphite plasma-facing wall, are in sharp contrast to recent studies on tokamaks with high-Z metallic walls, where frequent BZNs are found necessary to prevent radiative collapse of high-confinement, high-beta discharges [28,29]. When graphite is used as the plasma-facing surface, adequate wall conditions for high performance plasmas can be maintained over extended periods of operation without special wall conditioning. While BZN remains a useful tool to reduce impurity influx, especially oxygen, after an extended entry vent on DIII-D, repetitive use is found to be unnecessary. We note that these results are obtained with routine use of strong divertor pumping on DIII-D, which has been shown previously to maintain good wall conditions [30].

6. Conclusions

Recent experiments on DIII-D have extended the hybrid scenario towards the burning plasma regime by incorporating strong electron heating, low torque injection, and ELM suppression from RMPs. Using 2.4 MW of ECH to decrease T_i/T_e by ≈20% (bringing the volume-average

value down to ≈1.07) at fixed density and toroidal rotation, increases the measured turbulence at low and intermediate wavenumbers, and decreases H_{98y2} from 1.22 to 1.07. This is consistent with a calculated 50% increase in the maximum growth rate from the TGLF theory-based transport model. While reducing the injected torque using nearly balanced-NBI also yields moderate confinement factors (H_{98y2}≥1.1), such hybrid plasmas on DIII-D with q_{95}=3.1 still achieve conditions consistent with Q≥10 on ITER. In addition, hybrid scenario experiments on DIII-D contribute to the benchmarking of integrated simulation models for ITER [31]. For the first time, large type-I ELMs have been completely suppressed in hybrid plasmas with β_N up to 2.5 by applying edge RMPs using the DIII-D I-coil with toroidal mode number n=3. Finally, experiments on DIII-D have demonstrated the capability to obtain high performance plasmas, in both hybrid ($\beta_N H_{89}$~6) and steady-state (($\beta_N H_{89}$~9) scenarios, over extended operational periods (three months or >6000 plasma seconds) with no intervening boronizations with a >95% graphite plasma-facing wall.

Acknowledgments

This work was supported by the US Department of Energy under DE-FC02-04ER54698, DE-FG03-01ER54615, DE-AC52-07NA27344, DE-FG03-97ER54415, DE-FG02-89ER53296, DE-FG02-07ER54917, and DE-AC05-00OR22725.

References

[1] LUCE, T.C., *et al.*, Nucl. Fusion **41**, 1585 (2001).
[2] WADE, M.R., *et al.*, Phys. Plasmas **8**, 2208 (2001).
[3] SIPS, A.C.C., *et al.*, Plasma Phys. Controlled Fusion **44**, B69 (2002).
[4] JOFFRIN, E., *et al.*, Nucl. Fusion **45**, 626 (2005).
[5] ISAYAMA, A., *et al.*, Nucl. Fusion **43**, 1272 (2003).
[6] BURRELL, K.H., *et al.*, Plasma Physics and Controlled Nuclear Fusion Research (Proc. 13th Int. Conf. Washington, DC, 1990) (Vienna: IAEA) Vol. 1, p. 123.
[7] LUCE, T.C., *et al.*, Nucl. Fusion **43**, 321 (2003).
[8] WADE, M.R. *et al.*, Nucl. Fusion **45**, 407 (2005).
[9] PETTY, C.C., *et al.*, Phys. Rev. Lett. **83**, 3661 (1999).
[10] PETTY, C.C., LUCE, T.C., Phys. Plasmas **6**, 909 (1999).
[11] ITER PHYSICS BASIS, Nucl. Fusion **39**, 2175 (1999).
[12] St. JOHN, H., *et al.*, Plasma Physics and Controlled Nuclear Fusion Research (Proc. 15th Int. Conf. Seville, 1994) (Vienna: IAEA) Vol. 3, p. 603.
[13] GUPTA, D.K., *et al.*, Rev. Sci. Instrum. **75**, 3493 (2004).
[14] SCHMITZ, L., *et al.*, this conference.
[15] STAEBLER, G.M., *et al.*, Phys. Plasmas **14**, 055909 (2007).
[16] BURRELL, K.H., Phys. Plasmas **4**, 1499 (1997).
[17] BUTTERY, R.J., *et al.*, Phys. Plasmas **15**, 056115 (2008).
[18] POLITZER, P.A., *et al.*, Nucl. Fusion **48**, 075001 (2008).
[19] KINSEY, J.E., *et al.*, Phys. Plasmas **15**, 055908 (2008).
[20] PETTY, C.C., *et al.*, Fusion Sci. Technol. **43**, 1 (2003).
[21] EVANS, T.E., *et al.*, Nature Phys. **2**, 419 (2006).
[22] NAVE, M.F.F., WESSON, J.A., Nucl. Fusion **30**, 2575 (1990).
[23] LA HAYE, R.J., *et al.*, Nucl. Fusion **46**, 451 (2006).
[24] COLE, A.J., *et al.*, Phys. Rev. Lett. **99**, 065001 (2007).
[25] WEST, W.P., *et al.*, submitted to J. Nucl. Mater. (2008).
[26] WINTER, J., J. Nucl. Mater. **176-177**, 14 (1990).
[27] WEST, W.P., *et al.*, submitted to Plasma Phys. Control. Fusion (2008).
[28] LIPSCHULTZ, B., *et al.*, Phys. Plasmas **13**, 056117 (2006).
[29] NEU, R., *et al.*, J. Nucl. Mater. **363-365**, 52 (2007).
[30] MAINGI, R., *et al.*, Nucl. Fusion **36**, 245 (1996).
[31] KESSEL, C.E., *et al.*, Nucl. Fusion **47**, 1274 (2007).